DISSOLVED AND PARTICULATE ^{230}TH – ^{232}TH SYSTEMATICS IN THE CENTRAL EQUATORIAL PACIFIC OCEAN: EVIDENCE FOR FAR-FIELD TRANSPORT OF THE EAST PACIFIC RISE HYDROTHERMAL PLUME

A Thesis

by

GRECIA IVONNE LOPEZ

Submitted to the Office of Graduate and Professional Studies of
Texas A&M University
in partial fulfillment of the requirements for the degree of

MASTER OF SCIENCE

Chair of Committee,	Franco Marcantonio
Committee Members,	Ethan L. Grossman
	Mitchell Lyle
Head of Department,	John R. Giardino

August 2015

Major Subject: Geology

ABSTRACT

The goals of this thesis are to assess the distribution of ^{230}Th and ^{232}Th along a latitudinal gradient in the Central Equatorial Pacific Ocean (~155° W - 159°W) at two sites: 8°N and the equator. In so doing, I test for (1) the extent of advection or diffusion of dissolved ^{230}Th from the oligotrophic North Pacific gyre (low particle flux) to the more productive equatorial region (high particle flux), and (2) the efficacy of using ^{232}Th – ^{230}Th concentration systematics as a proxy for estimating dust fluxes to the sea surface in Central Equatorial Pacific Ocean. The dissolved ^{230}Th concentration profile at 8°N increases nearly linearly from the surface to 2000 m, exhibiting behavior consistent with thermodynamic reversible scavenging. However, from 2000 m to 3000 m, the dissolved ^{230}Th concentrations exhibit little change, before linearly increasing once more from 3000 m to the bottom. At this site dissolved ^{230}Th concentrations range from 1.1 fg/kg at 100 m to 55.2 fg/kg at 4600 m. At the equator, dissolved ^{230}Th concentrations are slightly lower, and range from undetectable at 25 m to 19.1 fg/kg at 3038 m. The pattern in the dissolved ^{230}Th concentration profile at the equator is indistinguishable from that at 8°N. The deep-water deviation from linearity between 2 and 3 km in the ^{230}Th profiles (lower concentrations than expected) at both sites occur in the interval of the water column that has the highest concentrations of ^{3}He and dissolved Fe. This ^{3}He- and Fe-rich signal has been traced to hydrothermal plumes from the EPR, thousands of km away. We hypothesize that the lower concentrations of ^{230}Th in mid-depth waters of the Central Equatorial Pacific are a result of scavenging of water-column ^{230}Th by Fe-Mn particulates

transported within the EPR hydrothermal plume during its 5000 km transit from the EPR to 160° W. Oceanic residence times of thorium combined with dissolved ^{232}Th concentrations suggest dust fluxes of about ~ 0.5 – 0.6 g m^{-2} yr^{-1} to the sea surface. These fluxes are in agreement with other empirical studies in the Pacific, but are higher than those suggested by global atmospheric circulation models.

DEDICATION

This thesis is dedicated to my family, my parents, Ana Jovel and Saul Lopez, for being a supportive force in my academic graduate career, especially my mother. My siblings: Carolina, Saul, and Jessica Lopez, for they have given me the strength, ability, and motivation to pursue my academic goals.

ACKNOWLEDGEMENTS

First and foremost, I would like to thank my research advisor, Dr. Franco Marcantonio, for he has supported me and believed in me more than I have believed in myself. There are not enough words to express my gratitude towards Dr. Marcantonio, he excels as an advisor, professor and friend and has guided me throughout the course of this research brilliantly. Through multiple discussions and projects, Dr. Marcantonio has shown me the advantages of a quantitative and analytical approach to research – namely efficiency of effort spent on solving, and richness in understanding of, research problems in radiogenic isotope geochemistry. Through the work done in this thesis, Dr. Marcantonio and I, show that through analytical and methodical treatment of isotopic seawater measurements, we are able to understand Th isotope dynamics and oceanic processes in the Central Equatorial Pacific Ocean. Furthermore, the research in this thesis expands upon Dr. Marcantonio's application and development of isotope and trace element geochemical proxies, and I am grateful for his teachings in radiogenic isotope geochemistry—Thorium isotope dynamics, for his time and contribution to the field of isotope and trace element geochemistry, and for the opportunity to contribute to his research.

Thanks also go to my friends and colleagues and the department faculty and staff for making my time at Texas A&M University a great experience. Especially Luz Romero, our Lab Manager, for her technical expertise, guidance, support and friendship throughout the course of my research.

Finally, thanks to my parents and siblings for their encouragement and to my best friend, Dr. Aaron Ames, for his patience, love and support.

NOMENCLATURE

CEP	Central Equatorial Pacific
EPR	Equatorial Pacific Rise
C_p	Particulate ^{230}Th concentrations
C_t	Total ^{230}Th concentrations

TABLE OF CONTENTS

Page

ABSTRACT ii

DEDICATION iv

ACKNOWLEDGEMENTS v

NOMENCLATURE vii

TABLE OF CONTENTS viii

LIST OF FIGURES x

LIST OF TABLES xi

1. INTRODUCTION 1

2. METHODOLOGY 4

2.1 Seawater and Sampling Collection 4
2.2 Radionuclide Analysis: Preparation and Column Chemistry 6

3. RESULTS 8

3.1 North Pacific Gyre: ML1208-12CTD 8
3.2 Equator: ML1208-03CTD 11
3.3 ^{232}Th Concentrations of the North Pacific Gyre and Equator 12

4. DISCUSSION 14

4.1 ^{230Th} Residence Time and Reversible Scavenging 14
4.2 Hydrothermal Plume and Effects on Dissolved ^{230}Th Concentrations between 2000 and 3000 m 21
4.3 Dissolved ^{230}Th Concentrations below 3000 m 26
4.4 Utilizing ^{232}Th – ^{230}Th Concentrations to Estimate Dust Flux and Lithogenic Input to the CEP 27
4.5 Dissolved Fe Fluxes based on ^{232}Th Fluxes 31

5. CONCLUSION 33

REFERENCES 35

LIST OF FIGURES

FIGURE Page

1. Water cast collection map 5

2. Filtered and unfiltered ^{230}Th concentrations in the Central Equatorial Pacific (Equator, and North Pacific Gyre) 10

3. Filtered and unfiltered ^{232}Th profiles of 8°N and the Equator..... 13

4. Total ^{230}Th profiles at 8°N 19

5. Total ^{230}Th profiles at 0°S 20

6. Excess ^{3}He and Dissolved Fe concentrations in the South Pacific replotted from Fitzsimmons et al. (2014)..... 24

7. Dissolved Fe concentrations replotted from Wu et al. (2011) (8°N, 158°W; 0°N, 158°W) in the CEP 25

LIST OF TABLES

TABLE Page

1. Water cast collected at 8°N 9

2. Water cast collected at 0°S 12

3. The scavenging residence times, sinking rate, and ^{230}Th depletions relative to reversible scavenging model prediction at each station 15

4. Dissolved ^{230}Th residence times and ^{232}Th Fluxes and Lithogenic Input for the CEP 30

1. INTRODUCTION

^{230}Th is widely used as a quantitative marine geochemical tracer due to its highly reactive chemical behavior. It is produced by the radioactive decay of ^{234}U ($T_{1/2}$ = 75.69 kyr), which is conservative in seawater and has a long residence time (~200 kyr; Cheng et al., 2000). ^{230}Th is essentially insoluble in seawater, so as it is produced it is quickly removed from the water column by adsorption onto particles which then settle to the seafloor. This process of adsorption and removal of ^{230}Th from the water column is called *scavenging*. ^{230}Th concentrations in seawater provide insight into oceanographic processes such as deep oceanic circulation and mixing rates, and marine particle dynamics (e.g., Nozaki and Horibe 1981; Van der Loeff and Berger, 1993; Moran et al., 1997). In addition, ^{230}Th studies of marine sediments provide important information on past changes in fluxes to the seafloor, which can be used to better understand climate-related changes in marine biological productivity, dust input to the oceans, and deep water circulation (e.g., Hayes et al., 2014) once the systematics are adequately understood.

Due to the quick scavenging of ^{230}Th by particles, the residence time of ^{230}Th in the ocean is approximately 10 - 40 years (Henderson and Anderson, 2003). It is assumed that the excess flux of Th carried to the seafloor by particles is equivalent to its rate of production (P_{Th}) by the decay of ^{234}U throughout the water column (Bacon, 1984; Francois et al., 2004; Henderson et al., 1999; Krishnaswami, 1976). Model simulations (Henderson et al., 1999; Marchal et al., 2000) and sediment trap studies (Scholten et al., 2005; Yu et al.,

2001) have been used to test this assumption, yielding the hypothesis that the flux of scavenged ^{230}Th (F_{Th}) to sediment at the seafloor remains within 30% of P_{Th} in 70% of the earth's oceans. If $F_{Th} = P_{Th}$, a linear increase in dissolved ^{230}Th concentration with depth in the water column is expected due to thermodynamic reversible exchange between dissolved and particulate ^{230}Th (Bacon and Anderson, 1982; Nozaki et al., 1981, 1987; Scholten et al., 2005; Van der Loeff and Berger, 1993; Moran et al., 1997, 2001, 2002). However, linear profiles are not as common as expected, and have been found only in some regions of the Southern Ocean (Van der Loeff and Berger, 1993), and the Central Pacific (Roy-Barman et al., 1996) and Northwestern Pacific (Nozaki et al., 1981) oceans. It is more common to find deviations from linearity. Such deviations indicate disturbance of the vertical equilibrium by lateral fluxes, or a change in the scavenging efficiency due to changes in particulate composition or flux (Hayes et al., 2014), and/or a failure of the assumption of equilibrium reversible scavenging.

Unlike the majority of ^{230}Th, which is supplied to the water column by the in-situ radioactive decay of ^{234}U, ^{232}Th ($T_{1/2}$ = 14 Ga; Holden, 1990) is derived from the leaching in open ocean waters of wind-blown dust from the continent. Indeed, such leaching provides approximately 99.8% of dissolved ^{232}Th to the open ocean water column (Santschi et al., 2006; Hayes et al., 2013a). When coupled with dissolved ^{230} Th analyses in the same water samples, dissolved ^{232}Th measurements offer a way to quantify the supply of dissolved ^{232}Th delivered by dust to the modern ocean (Deng et al., 2014; Hayes et al., 2013a; Hsieh et al., 2011). Such indirect measurements of the dust flux to the sea

surface, therefore, yield potential insights into the flux of dissolved Fe, an important limiting micronutrient supplied to the world's oceans via eolian processes (Jickells et al., 2005).

Here, we investigate the ^{230}Th and ^{232}Th depth profiles in the Central Pacific Basin. We find a non-linear profile with depth for ^{230}Th. We discuss several possibilities that can explain the non-linearity observed in the ^{230}Th profile, including: renewal of basin waters with different dissolved Th concentrations, recent mixing with depleted or enriched water masses, hydrothermal scavenging, and advection or diffusion of ^{230}Th in the water column (e.g. Anderson et al., 1983a, 1983b; Singh et al., 2013; Venchiarutti et al., 2008). In addition, we combine the systematics of dissolved ^{232}Th – ^{230}Th seawater concentrations to determine lithogenic input to the upper ocean in the CEP, and compare our results to others for the Pacific Ocean.

2. METHODOLOGY

2.1 Seawater and Sampling Collection

Seawater cast samples were taken from two sites in the Central Equatorial Pacific during an NSF-funded cruise to core the Line Islands Ridge in May 2012 (ML1208, on R/V Marcus Langseth). Five-liter samples at varying depths (24.5 – 4601 meters) were collected at 8°N, and at the equator using 24 PVC Niskin bottles mounted on a conductivity–temperature–depth (CTD) rosette system. The samples were collected to test for the extent of advection or diffusion of dissolved ^{230}Th from the oligotrophic North Pacific gyre to the more productive equatorial region, and the potential for water column scavenging (Broecker, 2008). We have assessed the distribution of total and dissolved ^{230}Th and ^{232}Th along a latitudinal gradient (~155° W - 159°W; Figure 1), from the equator to 8°N, an area that subsumes both low and high particle flux in the Central Equatorial Pacific. Sample ML1208-03CTD (00° 13.166’ S, 155° 57.668’ W) was collected at the equator whereas sample ML1208-12CTD was collected at the southern edge of the North Pacific gyre (8° 19.989’ N, 159° 18.000’ W).

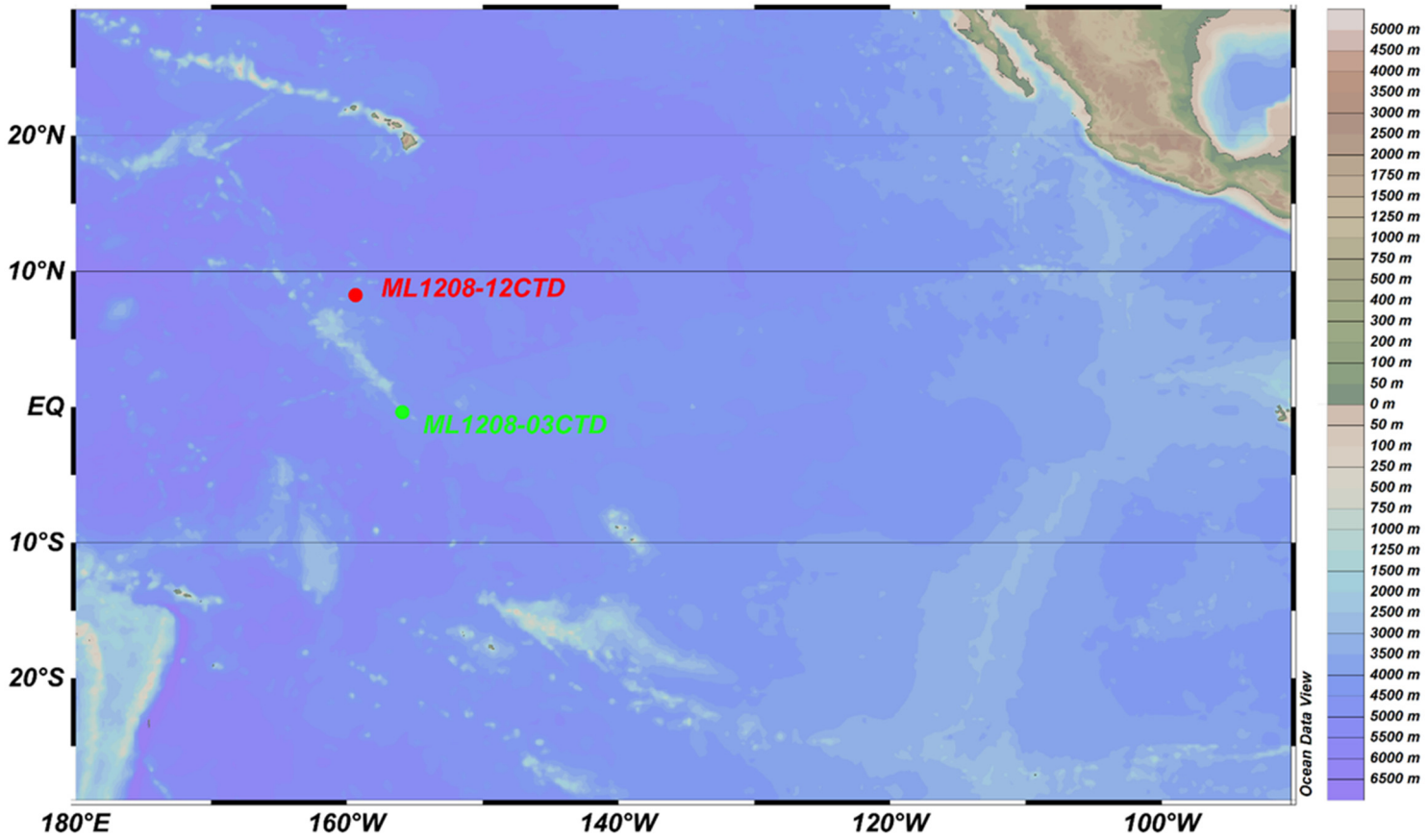

Figure 1. Water cast collection map. Line Islands, Central Equatorial Pacific. ML1208-03CTD (00° 13.166’ S, 155° 57.668’ W) and ML1208-12CTD (8° 19.989’ N, 159° 18.000’ W).

Collected seawater samples in PVC Niskin bottles were transferred via acid-washed Teflon tubing to prewashed 5-L polyethylene-collapsible cubitainers promptly after collection. Each cubitainer was rinsed with trace metal grade acid (10% HCl), cleansed three times with Milli-Q water, air-dried in a laminar airflow hood and stored separately inside the clean laboratory of the R. Ken Williams '45 Radiogenic Isotope Geosciences Laboratory at Texas A&M University. 0.45-mm Acropak filters were used to isolate the dissolved (filtered) fraction from the particulate (unfiltered) fraction during the transfer of seawater into the cubitainers. Prior to sampling, each cubitainer was washed with small amounts of seawater before the final transfer of the whole seawater sample. For all depths, 5-L filtered and 5-L unfiltered seawater samples were collected to study the dissolved and particulate ^{230}Th and ^{232}Th. Each sample was acidified with concentrated (9N) ultrapure (Optima-grade) HCl to a pH of approximately 1.5 and sent to Texas A&M University for radionuclide chemical analyses (Singh et al., 2013).

2.2 Radionuclide Analyses: Preparation and Column Chemistry

Using the revised protocol of the GEOTRACES program (Anderson et al., 2012) radionuclide measurements of total and dissolved ^{230}Th and ^{232}Th were evaluated. Water samples were weighed and spiked with ^{229}Th for isotope dilution analysis. To induce $Fe(OH)_3$ precipitation, a purified Fe-carrier solution ($FeCl_3$) was added. The iron chloride was purified by back extraction with isopropyl ether. After addition of the ^{229}Th spike and the $FeCl_3$ to the seawater sample, it was left to equilibrate for a day before the addition of trace metal-grade NH_4OH to bring the pH to 8-8.5. Once at desired pH, removal of all Th

and precipitation of iron hydroxide [$Fe(OH)_3$] within the seawater sample was achieved. The sample was left to equilibrate for 5 days, so the precipitate was able to settle undisturbed at the bottom of the cubitainer. After 5 days, the precipitate was separated from the supernatant solution through siphoning into 1 L acid-washed Nalgene bottles, and left to equilibrate for a full day. The following day, the sample was siphoned into acid-washed 50 mL centrifuge tubes, and placed in a centrifuge at 1700 rpm for 15 min. Samples were centrifuged three times, decanting the supernatant each time before dissolving the precipitate in ultrapure HNO_3. The resulting solution is then evaporated in an acid-washed 15 mL savillex beaker. Once evaporated the sample was reconstituted in 8N HNO_3. The sample solution was then processed through anionic ion-exchange columns (AG1X8, 100-200 mesh, chloride form) to purify and extract Th for isotope ratio measurement.

During column chemistry, each column was washed and conditioned (8N HNO_3, Milli-Q water, and concentrated HCl) before adding the sample. After each sample was added, the column was washed again, and a new acid-washed 15 mL beaker was placed to collect the Th (concentrated HCl is used during this step). Promptly after collecting Th, two drops of $HClO_4$ and 0.25 mL of concentrated HNO_3 were added and left to evaporate and fume on a hot plate at 180°. Once the solution reached 0.05 mL in volume, 2% HNO_3/0.1% HF was added and taken up to 1 mL of solution in 1.5 mL acid-washed centrifuge tubes for isotope ratio analysis on the Element XR magnetic sector ICP-MS. This allows us to obtain accurate and reliable quantitative ^{230}Th – ^{232}Th analyses at high resolution.

3. RESULTS

3.1 North Pacific Gyre: ML1208-12CTD

At 8°N, dissolved ^{230}Th concentrations range from 1.1 fg/kg at 100 m to 30.8 fg/kg at 4400 m, while dissolved ^{232}Th concentrations span from 10.2 pg/kg at 100 m to 19.7 pg/kg at 4400 m (Table 1, Figure 2 and Figure 3). The pattern of the dissolved ^{230}Th profile at 8°N is essentially linear from the surface to 2000 m. From 2000 m to 3000 m, the dissolved (filtered) ^{230}Th concentrations are constant, and then from 3000 m to the bottom, the profile is roughly linear above 1500 m, but noisier with a slightly differentiating slope from 1500 m to the bottom of the water column (Figure 2). At the same site, total ^{230}Th and ^{232}Th concentrations range from 1.1 fg/kg and 5.2 pg/kg, respectively, at 100 m to 55.2 fg/kg, 53.9 pg/kg, respectively, at 4600 m. (Table 1). The total (unfiltered) ^{230}Th profile mimics that of the dissolved ^{230}Th concentrations (Figure 2). The particulate fraction (filtered – unfiltered) of the total seawater ^{230}Th increases from about 0% at the surface to 38% at 4400 m (Table 1). From 0 to 3000 m at 8°N, dissolved ^{232}Th concentrations show little variability (~ 20%), suggesting a single source from the sea surface: likely, dissolution of eolian detrital material (Figure 3 and Table 1). From 3000 m to 4600 m, dissolved ^{232}Th contents are more variable and show a slight increase toward greater depths. The proportion of ^{232}Th in the particulate fraction of the total seawater sample increases exponentially with depth to a value of 56% in the bottommost sample (Figure 3), evidence for a deep nepheloid layer, perhaps sourced at the Line Islands Ridge

to the west. Due to errors in experimental procedure, we did not collect data for approximately nine samples (indicated by *, Table 1).

Water Cast ID: 8°N	Depth (m)	Filtered ^{230}Th (fg/kg)	Filtered ^{232}Th (pg/kg)	Unfiltered ^{230}Th (fg/kg)	Unfiltered ^{232}Th (pg/kg)	Particulate % ^{230Th} C_p/C_t (%)
ML1208-12CTD	100	1.095	10.160	1.056	5.175	-3.693
ML1208-12CTD	900	10.300	8.100	10.510	10.760	1.998
ML1208-12CTD	1500	18.900	11.700	18.540	13.617	-1.942
ML1208-12CTD	1800	18.620	8.364	22.540	10.314	17.391
ML1208-12CTD	2100	22.420	*	24.830	11.343	9.706
ML1208-12CTD	2400	22.600	8.800	25.660	10.722	11.925
ML1208-12CTD	2701	22.000	10.600	24.680	12.159	10.859
ML1208-12CTD	3001	22.030	19.500	*	*	*
ML1208-12CTD	3300	26.435	15.010	28.990	17.939	8.813
ML1208-12CTD	3600	*	*	32.330	138.982	*
ML1208-12CTD	3900	*	*	37.090	27.581	*
ML1208-12CTD	4201	29.000	16.700	41.220	32.308	28.646
ML1208-12CTD	4400	30.800	19.700	49.870	45.090	38.239
ML1208-12CTD	4601	*	*	55.150	53.861	*

Table 1. Water cast collected at 8°N. Shaded columns represent unfiltered Th; whereas the non-shaded columns of Th concentrations represent filtered values. Where Cp represents particulate ^{230}Th and Ct represents total ^{230}Th. Cp/Ct, represents the particulate fraction of total ^{230}Th (represented in % values).

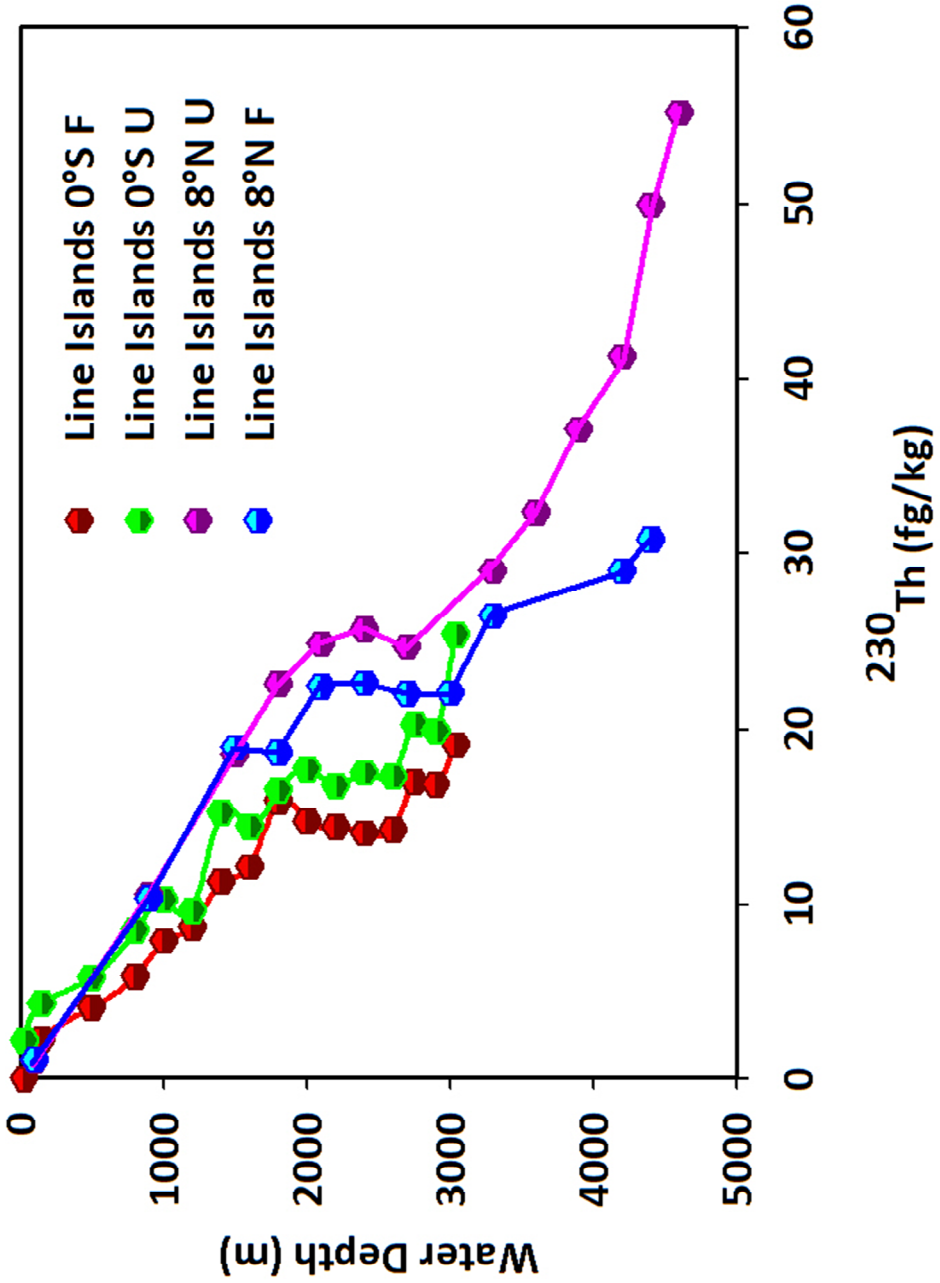

Figure 2. Filtered and unfiltered ^{230}Th concentrations in the Central Equatorial Pacific (Equator, and North Pacific Gyre). Plume induced anomalies as evidenced by a mid - depth depletion (2000 - 3000 m).

3.2 Equator: ML1208-03CTD

Thorium concentrations from the equator exhibit the same general trend that is exhibited at 8° N (North Pacific gyre). However, ^{230}Th values are not as high as those found at 8° N (Figure 2). Dissolved ^{230}Th concentrations range from not detectable at 25 m to 19.1 fg/kg at 3038 m of depth. The pattern of the dissolved ^{230}Th profile at 0° is essentially linear from the surface to 2000 m. Between 2000 m and 3000 m depth, dissolved ^{230}Th concentrations show little variability; beyond 3000 m depth, dissolved ^{230}Th concentrations increase with depth. Total ^{230}Th concentrations span from 2.2 fg/kg at 25 m to 25.4 fg/kg at 3038 m, while total ^{232}Th concentrations vary from 19.3 pg/kg at 25 m to 325.0 pg/kg at 3038 m (bottommost depth) (Table 2). As at 8°N, at equator profile of the total ^{230}Th concentrations mimic that of the dissolved ^{230}Th concentrations (Figure 2). The particulate fraction of the total seawater ^{230}Th ranges from about 100% at the surface to 24% at 3038 m (Table 2). There is a factor-of-two variability within the dissolved ^{232}Th concentrations, spanning from 3.9 pg/kg at 25 m to 8.1 pg/kg at 3038 m. Overall, however, there is no relationship of ^{232}Th concentrations with depth (Figure 3 and Table 2). The bottommost sample has an anomalously high total ^{232}Th concentration (Figure 3) and may reflect active resuspension of ^{232}Th-enriched fine-grained particles from the seafloor.

Water Cast ID: 0°N	Depth (m)	Filtered ^{230}Th (fg/kg)	Filtered ^{232}Th (pg/kg)	Unfiltered ^{230}Th (fg/kg)	Unfiltered ^{232}Th (pg/kg)	Particulate % ^{230}Th C_p/C_t (%)
ML1208-03CTD	25.4	0.000	3.857	2.177	19.344	100.000
ML1208-03CTD	147.6	2.265	12.806	4.317	29.707	47.533
ML1208-03CTD	499.5	4.096	6.193	5.780	17.492	29.135
ML1208-03CTD	801.1	5.850	6.051	8.500	30.196	31.176
ML1208-03CTD	1001.8	7.862	12.301	10.240	15.632	23.223
ML1208-03CTD	1200.3	8.660	5.770	9.634	16.562	10.110
ML1208-03CTD	1399.9	11.260	10.198	15.210	11.528	25.970
ML1208-03CTD	1600.5	12.130	5.956	14.430	19.363	15.939
ML1208-03CTD	1801	15.860	13.958	16.500	17.397	3.879
ML1208-03CTD	2001	14.710	12.932	17.700	25.320	16.893
ML1208-03CTD	2200	14.380	8.222	16.750	14.472	14.149
ML1208-03CTD	2401	14.050	6.880	17.490	14.262	19.668
ML1208-03CTD	2602	14.230	5.388	17.270	15.507	17.603
ML1208-03CTD	2749	16.960	7.145	20.224	24.203	16.139
ML1208-03CTD	2900	16.800	6.557	19.850	18.365	15.365
ML1208-03CTD	3038	19.070	8.090	25.390	325.015	24.892

Table 2. Water cast collected at 0°S. Shaded columns represent unfiltered Th; whereas the non-shaded columns of Th concentrations represent filtered values. Where Cp represents particulate ^{230}Th and Ct represents total ^{230}Th. Cp/Ct, represents the particulate fraction of total ^{230}Th (represent in % values).

3.3 ^{232}Th Concentrations at the North Pacific Gyre and Equator

Dissolved ^{232}Th profiles at both 8°N and the equator do not vary significantly with depth suggesting a single source from the sea surface: dissolution of eolian detrital material (Figure 3, Tables 1 and 2). Two anomalously-high ^{232}Th concentrations are found at similar depths in both transects, which may reflect involvement of a nepheloid layer that contains fine-grained lithogenic particles.

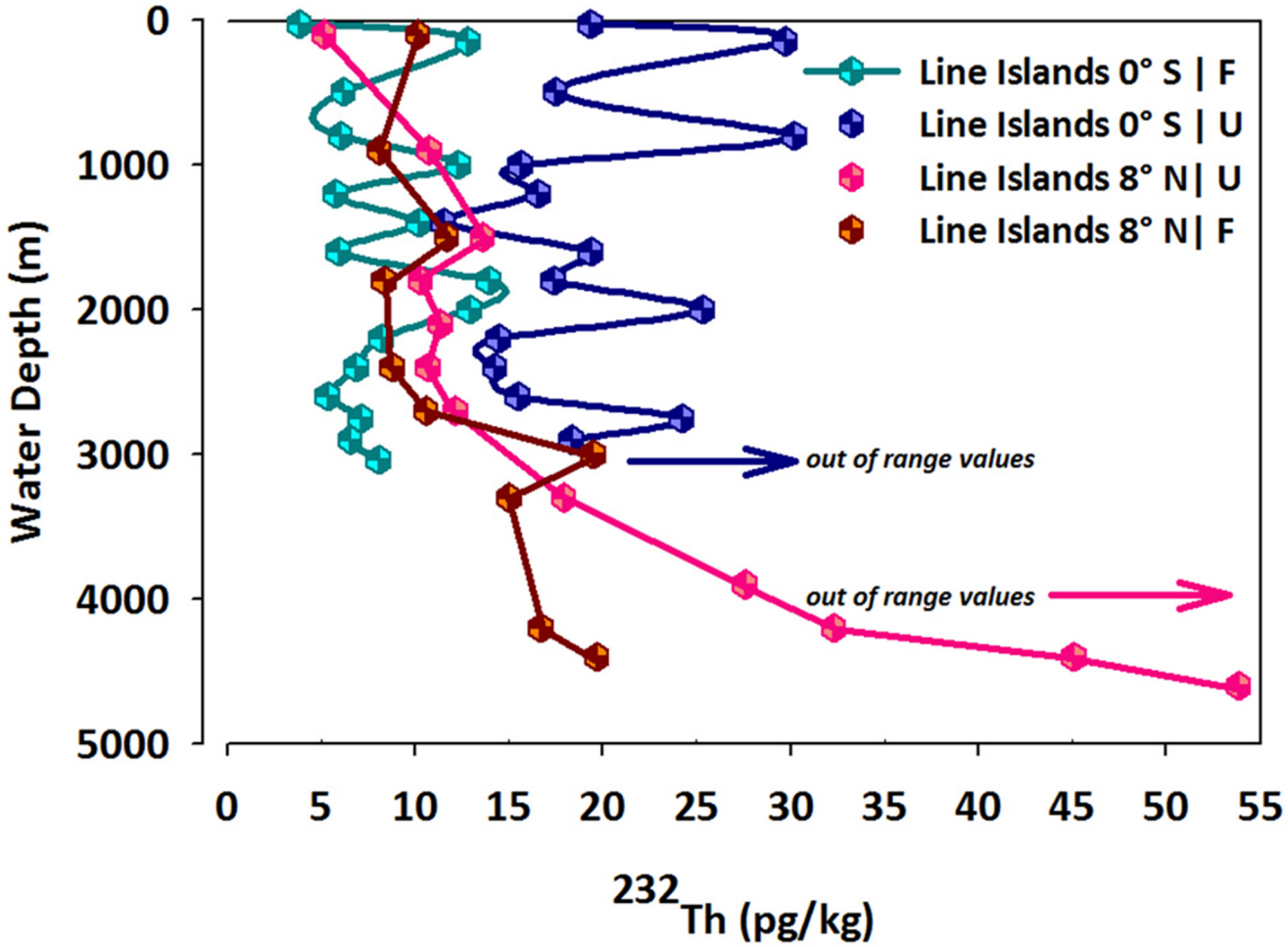

Figure 3. Filtered and unfiltered ^{232}Th profiles of 8°N and the Equator. Suggests for eolian dust deposition at both of our sites in the CEP.

4. DISCUSSION

4.1 ^{230}Th Residence Time and Reversible Scavenging

To provide further evidence for the behavior observed in our ^{230}Th profiles, we compare our ^{230}Th residence time values in the Central Equatorial Pacific to residence times calculated in other areas of the Pacific Ocean. We calculate total water column residence times for ^{230}Th at both of our sampling stations (00° 13.166' S, 155° 57.668' W; 8° 19.989' N, 159° 18.000' W). These calculations can be used to estimate the extent of depletion found within our ^{230}Th profiles relative to reversible scavenging. The first station (03CTD) is located at the equator where particle fluxes are greatest due to upwelling and high export particulate production. The second station (12CTD) is at 8°N and is within the oligotrophic North Pacific gyre where particulate fluxes are lower than those at the equator. We use the model found in Hayes et al. (2013a) to calculate residence times. Assuming no lateral transport, scavenging residence times of ^{230}Th were calculated using:

$$\frac{\int_{z0}^{zf} {}^{230}\mathrm{Th}(z)\,dz}{P_d z_f} \quad (1)$$

where the numerator represents the integrated inventory of total water column dissolved ^{230}Th, and the terms in the denominator, P_d and z_f, represent the production rate of thorium and the depth of the water column for each station, respectively.

The scavenging residence times of ^{230}Th for our equator and North Pacific sites are 16 and 31 years, respectively, within the range of oceanic ^{230}Th residence times recorded in the

Pacific Ocean (10 - 41 years, as summarized in Okubo et al., 2012; Nozaki et al., 1981; Anderson et al., 1983a, 1983b). The ^{230}Th residence time at the equator is lower by about a factor of 2 compared to the North Pacific site likely due to the higher scavenging efficiency of Th at the high-productivity equatorial site (Table 3).

Station	03CTD: Equator	12CTD: North Pacific gyre
Scavenging Residence time (yr)	16	31
Sinking rate (m/yr)	467	404
Depletion (%)	20	29

Table 3. The scavenging residence times, sinking rate, and ^{230}Th depletions relative to reversible scavenging model prediction at each station. The sinking rates were derived from the reversible scavenging model.

Throughout many of the world's ocean basins, ^{230}Th water column profiles are linear with depth suggesting reversible scavenging between dissolved and particulate ^{230}Th (Bacon and Anderson, 1982; Francois et al., 2004; Krishnaswami et al., 1976; Nozaki et al., 1981, 1987; Roy-Barman et al., 1996, 2009). Although linear increases of ^{230}Th concentrations with depth are observed at both of our sites from about 0-2000 m, this relationship breaks down at depths greater than 2000 m, as was also observed in the eastern Pacific by Singh

et al. (2013) and are found in the Bacon and Anderson (1982) profiles as well. The deviation from reversible scavenging below 2000 m is significant. To quantify the extent of deviation from reversible scavenging we construct a one-dimensional model in which equilibrium exists between adsorption/desorption reactions involving ^{230}Th in the dissolved phase and vertically sinking particles. In this simple model we assume that advection of ^{230}Th does not occur. The activity of total (particulate + dissolved) ^{230}Th, C_t, is given by (e.g., Krishnaswami et al., 1976; Anderson and Bacon, 1982; Van der Loeff and Berger, 1993; Moran et al., 1997; Okubo et al., 2012):

$$C_t = \left(\frac{P_d}{SK} z\right) \tag{2}$$

where P_d represents the production of ^{230}Th from ^{234}U decay in the water column (0.0267 dpm m^{-3} y^{-1}); S is the ^{230}Th particle settling rate (m y^{-1}); K is defined as the distribution coefficient of ^{230}Th between the particulate (unfiltered) and dissolved (filtered) phases; and depth, z, is measured in m. Particulate and dissolved data were used to determine the distribution coefficient K, which was calculated using total and dissolved ^{230}Th values. To determine particulate ^{230}Th, dissolved ^{230}Th was subtracted from the total ^{230}Th. For the North Pacific gyre an average K value of 0.13 was calculated; whereas for the equator a slightly higher average K value of 0.16 was determined. Both K values fall within the range of K values found in the Pacific Ocean (0.1 – 0.3; Bacon and Anderson, 1982; Nozaki et al., 1987; Okubo et al., 2007, 2012). Note that K correlates with the productivity behavior at each site—high K at the equator where there is high productivity and low K further north in the oligotrophic North Pacific. Indeed, this behavior is likely the cause of

the factor-of-two lower ^{230}Th residence time at the equator compared to 8°N. For equation (2), S can be approximated using measured total ^{230}Th, depth (z), and the constants P_d and K. S was calculated by fitting the calculated total ^{230}Th activity with the measured ^{230}Th activity for all water column depths and then taking the average. The settling rate values deduced in this way for the equator (467 m y^{-1}) and North Pacific gyre (404 m y^{-1}) are similar to others estimated in a similar fashion for the Pacific Ocean (380 m y^{-1} – 580 m y^{-1}; Bacon and Anderson, 1982; Nozaki et al., 1981, 1987; Okubo et al., 2007, 2012). The reversible scavenging model is not sensitive to the values of S making the approximation reasonable.

The distribution profiles of total ^{230}Th derived from the reversible scavenging model can be seen in Figure 4 and Figure 5 (solid black lines). The extent of anomalous depletion of ^{230}Th from a linear reversible scavenging profile can be calculated as follows:

$$\text{Depletion \%} = \frac{\int_{z0}^{zf}(\text{observed dissolved } ^{230}\text{Th}(z) - C_t(z))dz}{\int_{z0}^{zf} C_t\,(z)dz} \quad (3)$$

where the numerator is the integrated inventory of the difference between observed dissolved ^{230}Th and the total ^{230}Th predicted by the reversible scavenging model throughout the whole water column, and the denominator is the integrated inventory of total ^{230}Th. The depletion in ^{230}Th compared to reversible scavenging is clearly seen in Figures 1 and 2 below a depth of 2000 m. The quantitative extent of this depletion, from

about a depth of 2000 m to the bottom of the profile is similar at both the North Pacific Gyre (29%) and equator (20%) sites.

Depletions in ^{230}Th have been attributed to bottom scavenging (Bacon and Anderson, 1982; Nozaki and Nakanishi, 1985; Okubo et al., 2012; Singh et al., 2013; Hayes et al., 2013b), boundary scavenging (Bacon et al., 1976; Spencer et al., 1981; Anderson et al.,1983a, 1983b; Nozaki and Nakanishi, 1985; Cochran et al., 1987; Roy-Barman, 2009; Hayes et al., 2013b), renewal of basin waters with different dissolved Th concentrations (Francois et al., 2004; Hayes et al., 2014), enhanced scavenging of Th in high particle flux zones (Anderson et al., 1983a, 1983b; Bacon, 1988), recent mixing with depleted or enriched water masses (Van der Loeff and Berger, 1993; Scholten et al., 1995; Moran et al., 1995, 1997, 2002; Francois et al., 2004; Okubo et al., 2012; Hayes et al., 2013a, 2014), advection or diffusion of ^{230}Th in the water column (Nozaki et al., 1981; Bacon and Anderson, 1982; Van der Loeff and Berger, 1993; Chase et al., 2003; Venchiarutti et al., 2008; Singh et al., 2011), and/or hydrothermal scavenging (German et al., 1990, 1991; Kadko, 1994, 1996; Lupton, 1995, 1998; Hayes et al., 2014). In the CEP, we believe that the cause of the depletions in ^{230}Th that we observe is clearly hydrothermal in origin, and we present supporting evidence in the following sections.

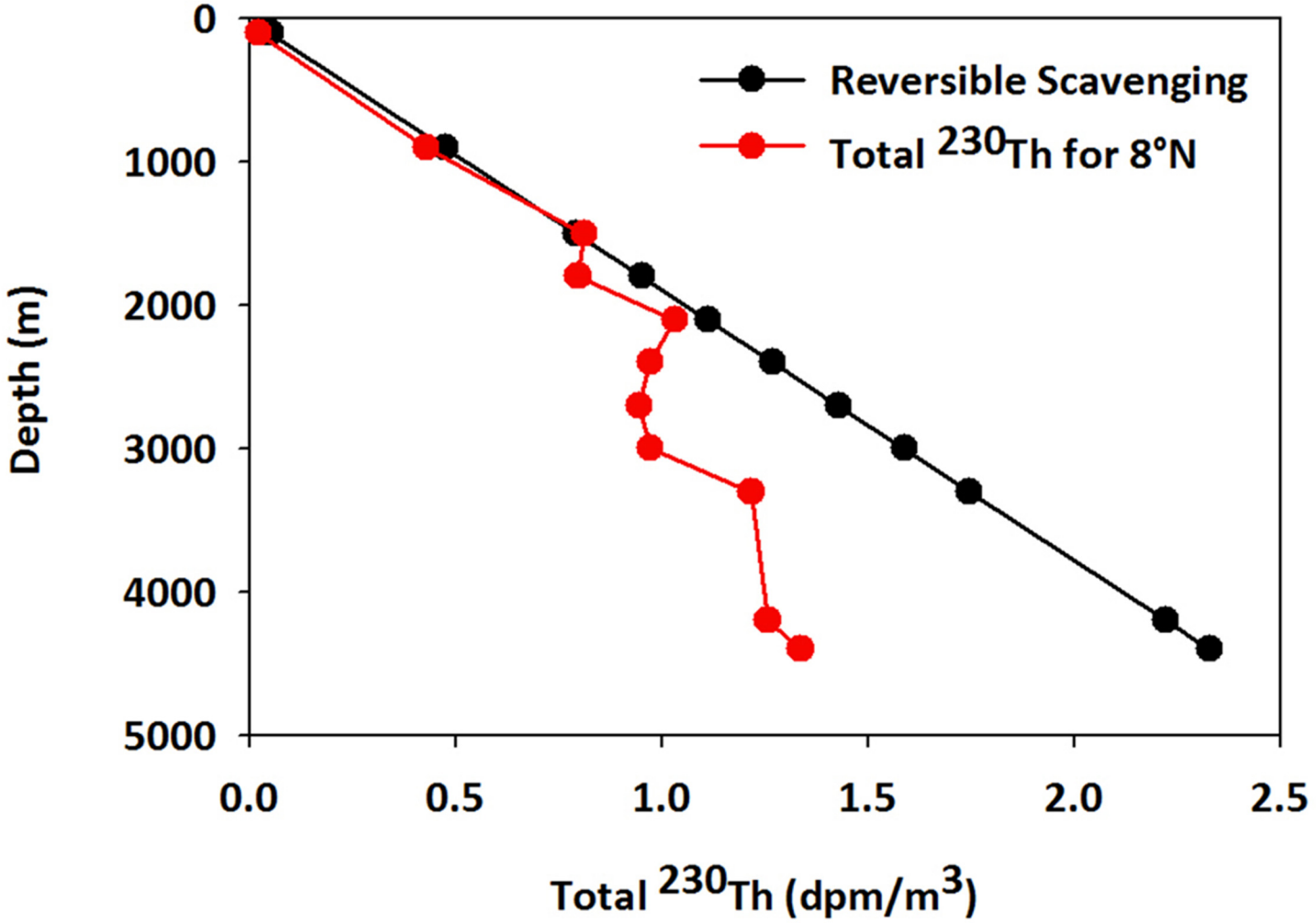

Figure 4. Total ^{230}Th profiles at 8°N. Red solid line represents our values. The black solid line represents the reversible scavenging model derived ^{230}Th distributions.

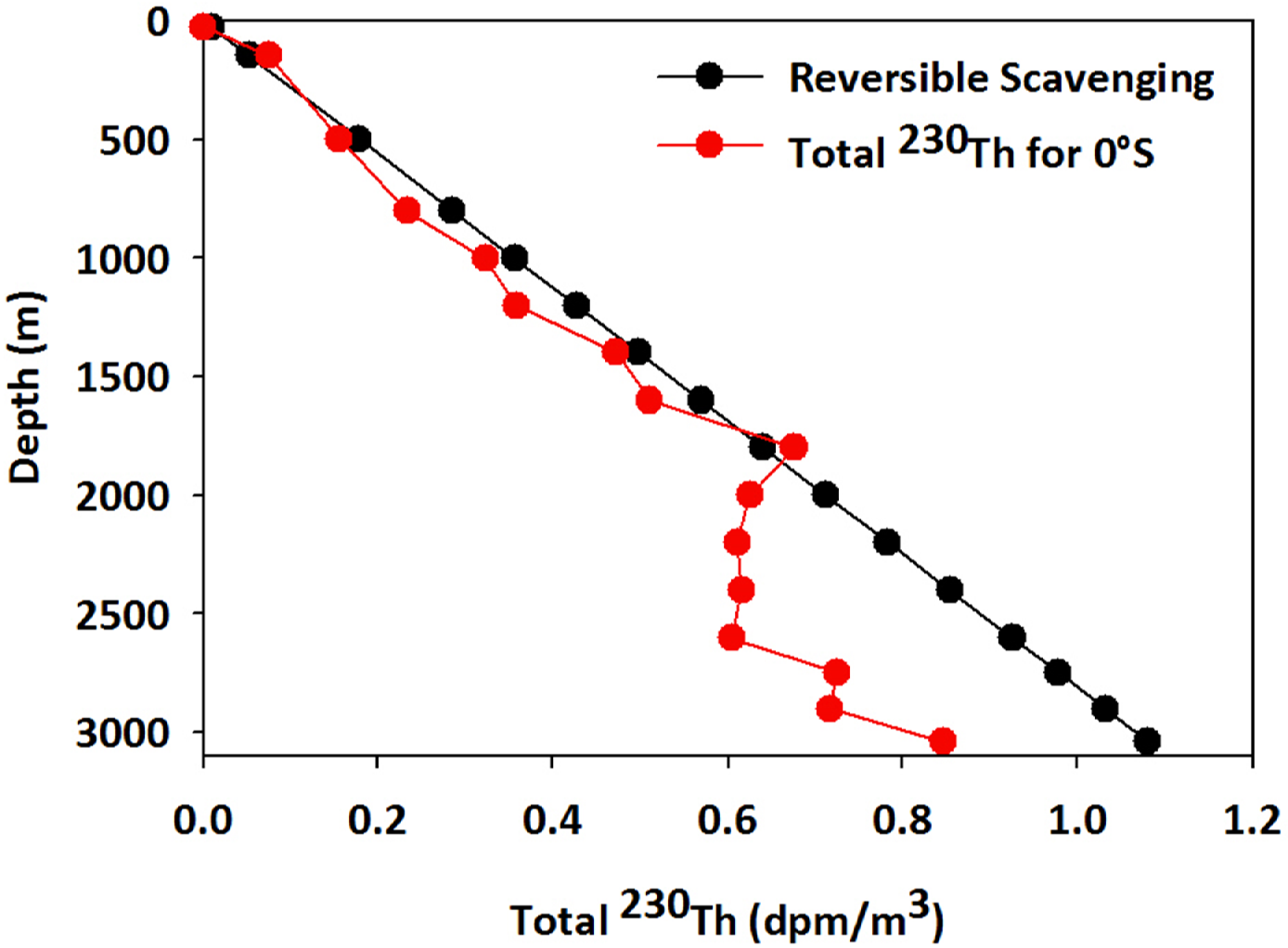

Figure 5. Total ^{230}Th profiles at 0°S. Our values are represented in the red solid line. The black solid line represents the reversible scavenging model derived ^{230}Th distributions.

4.2 Hydrothermal Plume and Effects on Dissolved ^{230}Th Concentrations between 2000 and 3000 m

Hydrothermal activity plays a vital role in the chemistry of the oceans—particularly in the Pacific Ocean, where ridge spreading is fast and voluminous. Emanation and subsequent dispersion of mantle ^{3}He from the EPR into deep ocean basins of the Pacific has been used to assess ocean circulation and mixing patterns (Lupton, 1998). In addition, radioisotopes have been used to quantify and effectively explore rates of chemical processes within hydrothermal plumes and the role these plumes play in the regulation of ocean chemistry (Kadko, 1996). Hydrothermal plumes are not only enriched in ^{3}He, but also in particulates enriched in metalliferous Mn and Fe. Such particulate plumes can be laterally transported from the ridge crest to the interior of oceans (e.g. Baker and Massoth, 1987; Kadko et al., 1990, 1996) and therefore affect the scavenging of trace elements (such as particle-reactive Th) within the water column (Dymond, 1981; Trocine and Trefry, 1988; Trefry and Metz, 1989; Feely et al., 1990; German et al., 1990, 1991; Kadko et al., 1994, 1996; Lupton, 1995, 1998;). Here, we assess whether such scavenging is the cause of the observed depletions in ^{230}Th below 2000 m at our sites that are more than 5,000 km away from the EPR (~110°W - 95°W).

To further support the idea that hydrothermal particulate scavenging of ^{230}Th can explain the trends in our Line Islands ^{230}Th profiles, we first need to evaluate evidence for migration of the EPR plume to the CEP. The first evidence for the far-field westward migration of the hydrothermal plume in the Pacific Ocean is the original ^{3}He concentration

data from the northern and southern Pacific Ocean from the Kermadec Trench (NOVA VI-2) and North Pacific (GEOSECS-I) stations, respectively (Clarke and Craig, 1969; Clarke and Craig, 1970; Craig et al., 1975). ^{3}He profiles far from the plume showed almost identical patterns, with the highest δ^{3}He values between depths of 2000 – 3000 m, and maxima at 2500 m (Clarke and Craig, 1969; Clarke and Craig, 1970; Craig et al., 1975). Since those first studies, other studies have shown similar profiles westward from the EPR throughout the Pacific Ocean (Lupton and Craig, 1981; Hudson et al., 1986; Klinkhammer and Hudson, 1986; German et al., 1991, 2002; Lupton, 1998; Lupton et al., 2004, Boyle and Jenkins, 2008; German and Seyfried, 2014). A recent synthesis of the ^{3}He data (German and Seyfried, 2014: their Figure 19) identifies the existence of two ^{3}He plumes with a maximum helium concentration at 2500 m, one centered between approximately 8° - 12°N north of the equator, and the other centered between about 15° - 5° S. If the ^{3}He data represent the true migration of the EPR hydrothermal plume, then manganese and iron profiles should be similar to those of helium. Indeed, this is the case (Klinkhammer and Hudson, 1986; Hudson et al., 1986; German et al., 1991; Wu et al., 2011; Fitzsimmons et al., 2014). Initial Mn work in the South Pacific showed dispersion patterns for hydrothermal Mn that suggests the existence of off-axis Mn anomalies at the same depths as helium anomalies originating from the EPR, and dispersed westward as far as ~2000 km (Klinkhammer and Hudson, 1986; Hudson et al., 1986; German et al., 1991). Complementary initial Fe data near the crest of the EPR at 19°S showed the same patterns in profile as those of Mn (Klinkhammer and Hudson, 1986; Hudson et al., 1986; German et al., 1991). More recent work with respect to both Fe and Mn has been

completed by Wu et al. (2011) and Fitzsimmons et al. (2014). Indeed, both studies found mid-depth Fe maxima (~2500 m) coincident with ^{3}He concentration maxima and profiles in tropical Pacific waters of the northern hemisphere (along 158°W and very close to our Line Islands sites; Wu et al., 2011) and the southern hemisphere (20°S, 170°W). These sites, respectively ~5000 km (Wu et al., 2011) and ~6000 km (Fitzsimmons et al., 2014) westward of the EPR hydrothermal vents, show similar profiles of Fe and ^{3}He concentrations between 2000 and 3000 m. More importantly our anomalous ^{230}Th depletions are the greatest between these same water depths (Figures 7 and 8) suggesting a significant role for non-equilibrium scavenging of particle-reactive nuclides by hydrothermal Fe-Mn particulates on a much larger Pacific-basin-wide scale than previously thought. Note that Wu et al. (2011) observed a lens of elevated dissolved Fe concentrations at depths of about 1000 – 2000 m observed by Wu et al. (2011) at the sites north of ours (20-25°N), which they attribute to an eastward dispersal of ^{3}He from the Loihi seamount located approximately 2000 km away from the study sites in the CEP (Lupton et al., 1998; Malahoff et al., 2006; Wu et al., 2011). ^{230}Th concentrations are low at such depths in the uppermost water column, and our sampling resolution is not high enough to resolve any depletions in thorium due to the Loihi hydrothermal particulate plume.

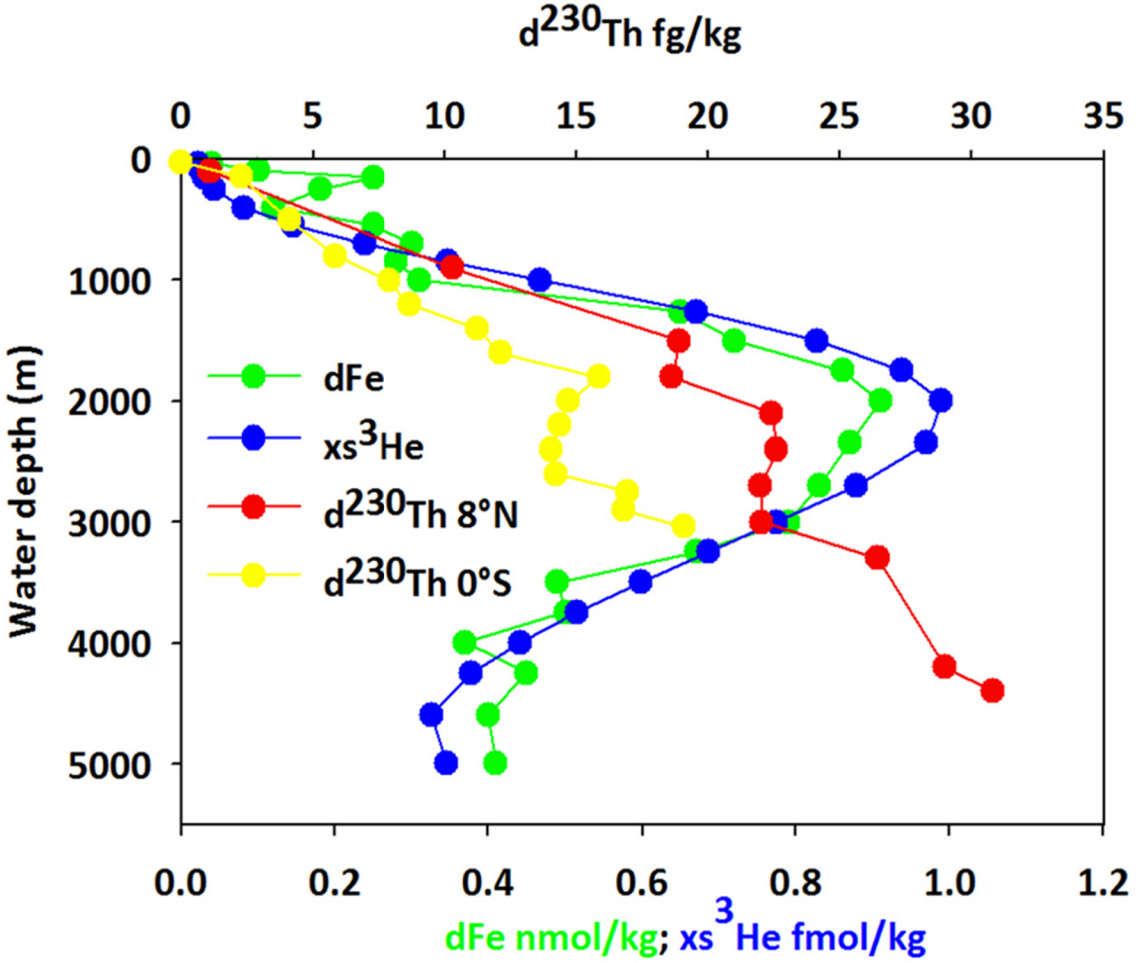

Figure 6. Excess ^{3}He and Dissolved Fe concentrations in the South Pacific replotted from Fitzsimmons et al. (2014) (20°S, 170°W). Measurements taken in the South Pacific were compared against our dissolved ^{230}Th concentration stations in the CEP.

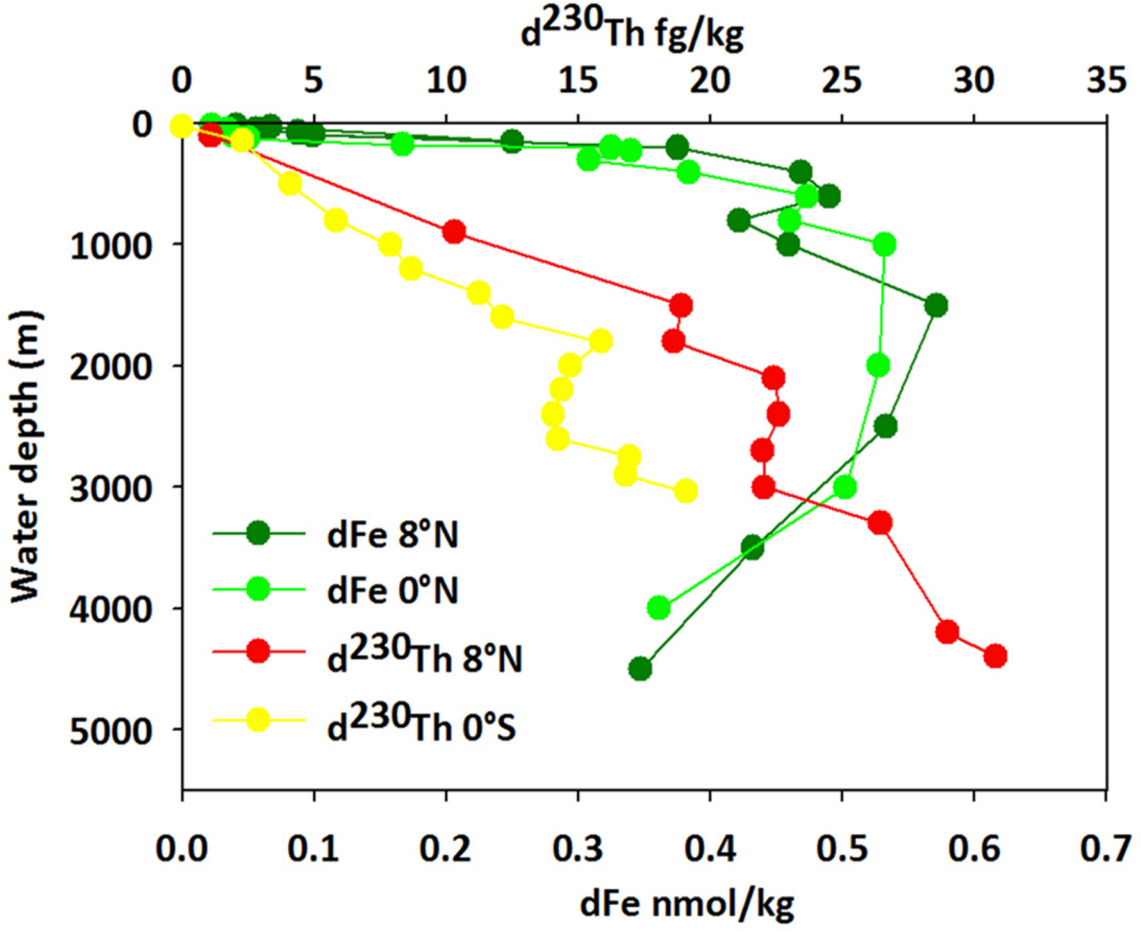

Figure 7. Dissolved Fe concentrations replotted from Wu et al. (2011) (8°N, 158°W; 0°N, 158°W) in the CEP. Because these measurements were taken at similar sites as our ^{230}Th dissolved concentrations in the CEP we compared our dissolved ^{230Th} values to those from Wu et al. (2011).

Contrary to previous studies, the notion that precipitation and sedimentation of particle-reactive metals occur relatively close to the ridge axis needs to be revisited. If our idea that the ^{230}Th depletion between 2000 and 3000 m is correct, then scavenging of particle-reactive elements by hydrothermal plume particulates *far* from the plume source needs to be included in models concerning the behavior of the elements in the ocean. Hydrothermal particulates are known to be deposited at these distances in the South Pacific, underneath the South Pacific ^{3}He plume (Lyle, 1986; Lyle et al., 1987). Although similar phenomena regarding scavenging of metals off-axis of hydrothermal fields are observed in the Arctic, Southern, and Atlantic Oceans (Klunder et al., 2011, 2012), the control exerted by the hydrothermal plume on trace metal behavior on such a vast scale (~5000 km) is only observed here in the Pacific Ocean basin.

4.3 Dissolved ^{230}Th Concentrations below 3000 m

Below 3000 m at the North Pacific gyre site, ^{230}Th concentrations increase and approach the reversible scavenging model ^{230}Th values. We believe this increase is evidence for deep water circulation along with downward mixing of low ^{230}Th waters from above 3000 m. Furthermore, as deep waters age and flow southwest in this region, ^{230}Th activities increase along their path. This gradual increase continues until steady – state distribution is reached and reversible scavenging behavior is regained (e.g., Francois et al., 2004; Hayes et al., 2014). There is evidence for a deep water mass (Circumpolar Deep Water—CDW) flowing eastward at approximately 15°N, traveling south on the west rim of the East Pacific Rise, and then westward towards the Equator (Johnson and Toole, 1993; Lyle

et al., 2014). It is these deep waters at our North Pacific gyre site which are mixing with the low-^{230}Th mid-depth waters, and regaining equilibrium toward higher ^{230}Th values.

4.4 Utilizing ^{232}Th – ^{230}Th Concentrations to Estimate Dust Flux and Lithogenic Input to the CEP

Wind-blown mineral aerosols (dust) contribute iron and other micronutrients to the surface ocean and therefore play an important role in the carbon cycle (e.g., Martin et al., 1990, 1991; Jickells et al., 2005; Winckler et al., 2008). In addition, dust affects the planet's radiative balance because of its role in the albedo (Watson et al., 2000; Jickells et al., 2005; Mahowald et al., 2006; Moore and Braucher, 2008; Wang et al., 2009). Quantifying the dust flux is challenging (Jickells et al., 2005; Hsieh et al., 2011), and dust input to the surface ocean has been assessed using remote sensing and modeling (Mahowald et al., 2005), combined with measurements of dissolved Al and Th concentrations in the surface ocean (Measures and Brown, 1996; Hsieh et al, 2011; Hayes et al., 2013a). Here we attempt to use dissolved concentrations of the primordial long-lived isotope ^{232}Th as an indicator of lithogenic input to the open ocean (e.g., Hsieh et al., 2011; Hayes et al., 2013a). In particular, estimating the supply of dust to the CEP will enhance our understanding of current dust models. Because the CEP is in such a remote region far from the blurring effects of the continental margins, dissolution of dust is the main source of dissolved ^{232}Th in the open ocean.

The advantage of using the thorium system is that the dissolved ^{230}Th concentration data can be used to constrain the flux of the dissolved ^{232}Th (the proxy for dust input).

Specifically, the supply of dissolved ^{230}Th in the water column can be determined by its rate of production through the decay of its parent ^{234}U which, in turn, allows us to calculate residence times for ^{230}Th with respect to its removal throughout the water column by scavenging. It is safe to assume that ^{230}Th and ^{232}Th have the same residence time, since ^{232}Th and ^{230}Th are isotopes of the same element. Hence, the removal rate of dissolved ^{232}Th within an interval of the water column can be calculated by dividing the measured inventory of ^{232}Th by the ^{230}Th residence time within the same interval. The interval of the water column from 0-500 m has been argued by Hayes et al. (2013a) to be the most affected by dust input to the surface ocean, and we follow their methodology here.

Assuming steady state for the top 500 m, the scavenging removal rate of ^{230}Th or ^{232}Th is equal to the inverse of the ^{230}Th residence time, τ_{Th}, and can be calculated using the measured dissolved ^{230}Th concentrations from each station in the CEP, and comparing it to the production of ^{230}Th by ^{234}U decay within the same interval. Once the 500-m ^{230}Th residence time is calculated, it is applied to the integrated inventory of dissolved ^{232}Th in order to approximate the ^{232}Th flux due to mineral dust dissolution from 0 to 500 m (Hirose and Sugimura, 1987; Hayes et al., 2013a). As described by Hsieh et al. (2011) and Hayes et al. (2013a), in order to estimate the lithogenic flux, the concentration of dissolved ^{232}Th, $[^{232}Th]_{litho}$, and its fractional solubility, S_{Th}, are necessary (see equation 4). Note, for the North Pacific Gyre, a linear interpolation was necessary to determine the dissolved ^{230}Th and ^{232}Th concentrations at 500 m. Such an interpolation is justified for ^{230}Th given its reversible behavior to 2000 m. For ^{232}Th, there is little variability

with depth.

$$\text{Lithogenic Flux (z)} = \frac{\int_{z0}^{zf} \text{Dissolved } ^{232}\text{Th dz}}{\tau^{230}\text{Th(z)} * [^{232}\text{Th}]_{\text{litho}} * S_{\text{Th}}} \quad (4)$$

The residence times of the ^{230}Th in the top 500 m at the Equator and North Pacific Gyre sites are approximately 3.3 and 4.1 years, respectively. These surface-ocean ^{230}Th residence times are similar to residence times found in Luo et al. (1995), Hayes et al. (2013a) and Deng et al. (2014). Residence times calculated in Luo et al. (1995), were calculated for sites closest to ours: 4.2 years at 9°N, 140°W and 3.9 years at 2°S, 140°W. While similar to our sites, the integration depth in Luo et al. (1995) was the surface to 100 m. Hayes et al. (2013a) chose an integration depth of 0 – 500 m, and found Th residence times in the North Pacific between 3.7 – 6.4 years, consistent with the values found at our sites in the CEP. With regard to dissolved ^{232}Th fluxes, approximations of the concentrations and fractional solubility of ^{232}Th in the dust are essential. Most studies suggest normalizing ^{232}Th lithogenic concentrations to an averaged upper continental crust value of 10.7 ppm (Taylor and McLennan, 1995; McGee et al., 2007; Winckler et al., 2008; Woodard et al., 2012). Fractional solubility of Th in dust, S_{Th}, is more difficult to assess. We have utilized an estimated value of 20% that falls within the range of previous studies (Arraes-Mescoff et al., 2001; Roy-Barman et al., 2002; Hsieh et al., 2011; Hayes et al., 2013a). Calculated removal fluxes for ^{232}Th range from 1.1 – 1.4 μg m^{-2} yr^{-1} for the upper ocean in the Central Equatorial Pacific (Table 4). Central Equatorial Pacific dust deposition estimates determined via integration of ^{232}Th inventories from 0 – 500 m are approximately 0.6 g m^{-2} yr^{-1} (Table 4), and complement the values for the subtropical North Pacific estimated by Hayes et al. (2013). The low dust fluxes observed are consistent

with the remote location of the CEP. We can also compare our 500-m dissolved ^{232}Th dust flux values to dust deposition estimates from marine sediments. For the Holocene period, rates of supply of dust delivered to the equatorial Pacific seafloor range from 0.13 – 0.55 g m^{-2} yr^{-1} (Winckler et al., 2008). Our values are on the high end of those estimated by Winckler et al. (2008) for dust deposition at 140°W. Our empirical estimate and that of Winckler et al. (2008) are lower than estimates given by dust models for the equatorial Pacific for which dust fluxes span from 0.01 – 0.1 g m^{-2} yr^{-1} (Figure 2 in Mahowald et al., 2005).

Station	τ^{230}Th (500 m, years)	^{232}Th flux (µg m^{-2} yr^{-1})	Dissolved Th derived Lithogenic Flux (g m^{-2} yr^{-1}) S_{Th} = 20%; 500 m	Dissolved Fe Flux (g Fe m $^{-2}$yr^{-1})
ML1208-03CTD: Equator	3.3	1.4	0.6	0.0186
ML1208-12CTD: N. Pacific Gyre	4.1	1.1	0.5	0.0155

Table 4. Dissolved ^{230}Th residence times and ^{232}Th Fluxes and Lithogenic Input for the CEP. Calculated via depth integration of 0 - 500 m via Hsieh et al. (2011) and Hayes et al. (2013) approach**.**

4.5 Dissolved Fe Fluxes based on ^{232}Th Fluxes

The supply of Fe can be determined by estimating the ratio of the partial dissolution of Fe to Th in the dust (S_{Fe}/S_{Th}), and by assuming an average Fe/Th concentration ratio in the dust that is equal to the mole ratio in the continental crust (A_{Fe}/A_{Th}). The dissolved Fe supply to the sea surface can then be estimated as follows:

$$\text{Dissolved Fe Supply} = \text{Dissolved } ^{232}\text{Th flux} * (A_{Fe}/A_{Th}) * (S_{Fe}/S_{Th}) \quad (5)$$

Application of equation (5) results in dissolved Fe fluxes of approximately 15.5 (North Pacific Gyre) to 18.6 mg Fe $m^{-2}yr^{-1}$ (Equator) in the CEP (Table 4), using our estimated dissolved ^{232}Th fluxes in Table 4. We assume the same values used by Hayes et al. (2014) for A_{Fe}/A_{Th} (13,553 mol/mol) and S_{Fe}/S_{Th} (1). Our dissolved Fe fluxes are comparable to those estimated at the INOPEX sites in the North Pacific (15 mg Fe $m^{-2}yr^{-1}$) by Hayes et al. (2013a). When compared to model-derived estimates of Fe deposition in Mahowald et al. (2009), our values in the CEP as well as the INOPEX North Pacific values in Hayes et al. (2013a) are about a factor of 2 higher (model results yield estimates of about 5–10 mg Fe $m^{-2}yr^{-1}$).

Although Pacific model dust and Fe fluxes are lower than those estimated empirically by us and Hayes et al. (2013a), using similar thorium systematics, Hsieh et al. (2011) measured dust fluxes in the Atlantic that agree with those modeled by Mahowald et al. (2005). The agreement between Atlantic dust models and measurements may be due to the high supply of dust to the Atlantic that makes measurements easier and models more robust. On the other hand, in the Pacific, the miniscule amounts of dust delivered to the

oceans magnify the inherent errors. Sensitivity to S_{Th} and, therefore, S_{Fe}/S_{Th}, could also explain the factor of 2 difference between models and measurements in the Pacific. If that were the case, then either S_{Th} would have to be a factor of 2 higher, the S_{Fe}/S_{Th} would have to be double what is assumed, or a combination of the two would need to be invoked. Whether such changes are likely can only be determined upon experimental determination of solubilities of Th and Fe dust, which has yet to take place. For the time being, we are faced with an uncertainty of a factor of two difference between empirical estimates and models. Clearly, further research is required in order to apply long-lived Th isotopes as a quantitative tool to estimate the supply of trace elements from lithogenic sources to the upper ocean.

5. CONCLUSION

Low concentrations of ^{230}Th at the equator and 8°N in central equatorial Pacific Basin mid-depth (2000-3000 m) waters result from far – field hydrothermal scavenging by a hydrothermal plume emanating from the East Pacific Rise approximately 5000 km away from our sites. This is further supported by dissolved Fe, dissolved Mn and ^{3}He studies conducted in the near vicinity of our study area, which suggest that these hydrothermal vent fluids and particulates have retained their signature throughout the lifetime of the plume and have traveled ~ 5000 km westward to our sites. The plume significantly contributes to the removal of ^{230}Th and, likely, other particle – reactive trace elements on a basin – wide scale in the CEP.

Reversible scavenging explains the behavior observed in the upper 2000 m of our ^{230}Th profiles at the equator and North Pacific gyre. ^{230}Th concentrations linearly increase with depth until 2000 m and stay constant between 2000-3000 m. This 1000-m mid-depth interval correlates with high ^{3}He and Fe-Mn concentrations that are a signature of a hydrothermal plume extending from the EPR. While depths for the equator profile ends at ~3000 m, the North Pacific gyre ^{230}Th concentrations below 3000 m are consistent with deep water circulation and mixing behavior. ^{230}Th-depleted water resulting from mid-depth hydrothermal scavenging mixes with southwestward flowing circumpolar deep water. The mixing produces ^{230}Th activities in the deepest waters that gradually increase and approach the reversible scavenging model concentrations.

Finally, our dissolved ^{232}Th concentrations are relatively invariable with depth throughout the water column for both sites, suggesting dissolution of dust in the upper ocean. In addition, by combining our measured seawater ^{232}Th – ^{230}Th concentrations within the topmost water column, as done in recent studies (Hsieh et al., 2011; Hayes et al., 2013; Deng et al., 2014), we were able to determine dissolved ^{232}Th lithogenic fluxes to be between 0.5 – 0.6 g m^{-2} yr^{-1} in the CEP. While dust flux should be relatively low in the CEP due to its remote location, our values suggest that model – derived dust fluxes calculated by Mahowald et al. (2005) and Jickells et al. (2005) (0.01 – 0.1 g m^{-2} yr^{-1}) underestimate dust deposition in the Pacific by a factor of two.

REFERENCES

Anderson, R. F., Bacon, M. P., Brewer, P. G. (1983a). Removal of ^{230}Th and ^{231}Pa from the open ocean. *Earth and Planetary Science Letters*, 62(1), pp. 7-23.

Anderson, R. F., Bacon, M. P., Brewer, P. G. (1983b). Removal of ^{230}Th and ^{231}Pa at ocean margins. *Earth and Planetary Science Letters*, 66, pp. 73-90.

Anderson, R. F., Lao, Y., Broecker, W. S., Trumbore, S. E., Hofmann, H. J., Wolfli, W. (1990). Boundary scavenging in the Pacific Ocean: a comparison of ^{10}Be and ^{231}Pa. *Earth and Planetary Science Letters*, 96, pp. 287-304.

Anderson, R. F., Fleisher, M. Q., Robinson, L. F., Edwards, R. L., Hoff, J., Moran, S. B., Rutgers van der Loeff, M. M., Thomas, A. L., Roy-Barman, M., François, R. (2012). GEOTRACES intercalibration of ^{230}Th, ^{232}Th, ^{231}Pa, and prospects for ^{10}Be. *Limnology Oceanography Methods*, 10, pp. 179-213.

Arraes-Mescoff, R., Roy-Barman, M., Coppola, L., Souhaut, M., Tachikawa, K., Jeandel, C., Sempere, R., Yoro, C. (2001). The behavior of Al, Mn, Ba, Sr, REE and Th isotopes during in vitro degradation of large marine particles. *Marine Chemistry*, 73, pp. 1-19.

Bacon, M. P., Spencer, D. W., Brewer, P.G. (1976). ^{210}Pb/^{226}Ra and ^{210}Po/^{210}Pb disequilibria in seawater and suspended particulate matter. *Earth and Planetary Science Letters*, 32, pp. 277-296.

Bacon, M. P., Anderson, R. F. (1982). Distribution of thorium isotopes between dissolved and particulate forms in the deep sea. *Journal of Geophysical Research*, 87, pp. 2045-2056.

Bacon, M. P. (1984). Glacial to interglacial changes in carbonate and clay sedimentation in the Atlantic Ocean estimated from ^{230}Th measurements. *Chemical Geology*, 46, pp. 97-111.

Bacon, M. P. (1988). Tracers of chemical scavenging in the ocean: boundary effects and large-scale chemical fractionation. *Philosophical Transactions of the Royal Society London A Mathematical Physical and Engineering Sciences Journal*, 325(1583), pp. 147-160.

Baker, E. T., Massoth, G. J. (1987). Characteristics of hydrothermal plumes over two vent fields on the Juan de Fuca Ridge, northeast Pacific Ocean. *Earth and Planetary Science Letters*, 85, pp. 59-73.

Boyle, E., Jenkins, W. (2008). Hydrothermal iron in the deep western South Pacific. *Geochimica et Cosmochimica Acta Supplement*, 72, pp. 107.

Broecker, W. (2008). Excess sediment ^{230}Th: transport along the sea floor or enhanced water column scavenging? *Global Biogeochemical Cycles*, 22, GB1006.

Chase, Z., Anderson, R. F., Fleisher, M. Q., Kubik, P. W. (2003). Scavenging of ^{230}Th, ^{231}Pa and ^{10}Be in the Southern Ocean (SW Pacific sector): the importance of particle flux, particle composition and advection. *Deep Sea Research Part II: Topical Studies in Oceanography*, 50(3), pp. 739-768.

Cheng, H., Edwards, R. L., Hoff, J., Gallup, C. D., Richards, D. A., Asmerom, Y. (2000). The half-lives of uranium-234 and thorium-230. *Chemical Geology*, 169, pp. 17-33.

Clarke, W. B., Beg, M. A., Craig, H. (1969). Excess ^{3}He in the sea: Evidence for terrestrial primodal helium. *Earth and Planetary Science Letters*, 6(3), pp. 213-220.

Clarke, W. B., Beg, M. A., Craig, H. (1970). Excess helium-3 at the North Pacific Geosecs station. *Journal of Geophysical Research*, 75(36), pp. 7676-7678.

Cochran, J. K., Livingston, H. D., Hirschberg, D. J., Surprenant, L. D. (1987). Natural and anthropogenic radionuclide distributions in the Northwest Atlantic Ocean. *Earth and Planetary Science Letters*, 84, pp. 135-152.

Craig, H., Clarke, W. B., Beg, M. A. (1975). Excess ^{3}He in deep water on the East Pacific Rise. *Earth and Planetary Science Letters*, 26(2), pp. 125-132.

Deng, F., Thomas, A. L., Rijkenberg, M. J., Henderson, G. M. (2014). Controls on seawater ^{231}Pa, ^{230}Th and ^{232}Th concentrations along the flow paths of deep waters in the Southwest Atlantic. *Earth and Planetary Science Letters*, 390, pp. 93-102.

Dymond, J. (1981). Geochemistry of Nazca plate surface sediments: An evaluation of hydrothermal, biogenic, detrital and hydrogenous sources. *Geological Society of America Memoirs*, 154, pp. 133-173.

Feely, R. A., Massoth, G. J., Baker, E. T., Cowen, J. P., Lamb, M. F., and Krogslaud, K. A. (1990). The effect of hydrothermal processes on midwater phosphorous distributions in the northeast Pacific. *Earth and Planetary Science Letters*, 96, pp. 305-318.

Fitzsimmons, J. N., Boyle, E. A. and Jenkins, W. J. (2014). Distal transport of dissolved hydrothermal iron in the deep South Pacific Ocean. *Proceedings of the National Academy of Sciences*, 111(47), pp. 16654-16661.

François, R., Frank, M., Rutgers van der Loeff, M. M., Bacon, M. P. (2004). ^{230}Th normalization: an essential tool for interpreting sedimentary fluxes during the late Quaternary. *Paleoceanography*, 19, PA1018.

German, C. R., Klinkhammer, G. P., Edmond, J. M., Mitra, A., and Elderfield, H. (1990). Hydrothermal scavenging of rare Earth elements in the ocean. *Nature*, 345, pp. 516-518.

German, C. R., Fleer, A. P., Bacon, M. P., and Edmond, J. M. (1991). Hydrothermal scavenging at the Mid-Atlantic Ridge: Radionuclide distributions. *Earth and Planetary Science Letters*, 105, pp. 170-181.

German, C. R., Colley, S., Palmer, M. R., Khripounoff, A., and Klinkhammer, G. P. (2002). Hydrothermal plume-particle fluxes at 13°N on the East Pacific Rise. *Deep Sea Research Part I: Oceanographic Research Papers*, 49(11), pp. 1921-1940.

German, C. R. and Seyfried, W. E. (2014). *8.7 - Hydrothermal Processes*. In: K.K. Turekian and H.D. Holland (Editors), Treatise on Geochemistry (Second Edition). Elsevier, Oxford, pp. 191-233.

Hayes, C. T., Anderson, R.F., Fleisher, M.Q., Serno, S., Winckler, G., Gersonde, R. (2013a). Quantifying lithogenic inputs to the North Pacific Ocean using the long-lived thorium isotopes. *Earth and Planetary Science Letters*, Volume 383, pp. 16-25.

Hayes, C. T., Anderson, R. F., Jaccard, S. L., François, R., Fleisher, M. Q., Soon, M., Gersonde, R. (2013b). A new perspective on boundary scavenging in the North Pacific Ocean. *Earth and Planetary Science Letters*, 369, pp. 86-97.

Hayes, C. T., Anderson, R. F., Fleisher, M. Q., Huang, K. F., Robinson, L. F., Lu, Y., and Moran, S. B. (2014). ^{230}Th and ^{231}Pa on GEOTRACES GA03, the US GEOTRACES North Atlantic transect, and implications for modern and paleoceanographic chemical fluxes. *Deep Sea Research Part II: Topical Studies in Oceanography*, in press.

Hirose, K. and Sugimura, Y. (1987). Thorium isotopes in the surface air of the western North Pacific Ocean. *Journal of Environmental Radioactivity*, 5, pp. 459-475.

Henderson, G. M., Anderson, R. F. (2003). The U-series toolbox for paleoceanography. *Reviews in Mineralogy and Geochemistry*, 52, pp. 493-531.

Henderson, G. M., Heinze, C., Anderson, R. F., Winguth, A. M. E. (1999). Global distribution of the ^{230}Th flux to ocean sediments constrained by GCM modelling. *Deep Sea Research Part I: Oceanographic Research Papers*, 46(11), pp. 1861-1893.

Holden, N. E. (1990). Total half-lives for selected nuclides. *Pure and Applied Chemistry*, 62, pp. 941-958.

Hsieh, Y. T., Henderson, G. M., Thomas, A. L. (2011). Combining ^{232}Th and ^{230}Th concentrations to determine dust fluxes to the surface ocean. *Earth and Planetary Science Letters*, 312(3-4), pp. 280-290.

Hudson, A., Bender, M. L., & Graham, D. W. (1986). Iron enrichments in hydrothermal plumes over the East Pacific Rise. *Earth and Planetary Science Letters*, 79(3), pp. 250-254.

Jickells, T. D., An, Z. S., Andersen, K. K., Baker, A. R., Bergametti, G., Brooks, N., Cao, J. J., Boyd, P. W., Duce, R. A., Hunter, K. A., Kawahata, H., Kubilay, N., laRoche, J., Liss, P. S., Mahowald, N., Prospero, J. M., Ridgwell, A. J., Tegen, I., Torres, R. (2005). Global iron connections between desert dust, ocean biogeochemistry, and climate. *Science*, 308, pp. 67-71.

Johnson, G. C., and Toole, J. M. (1993). Flow of deep and bottom waters in the Pacific at 10°N. *Deep Sea Research Part I: Oceanographic Research Papers*, 40(2), pp. 371-394.

Kadko, D., Rosenberg, N. D., Lupton, J. E., Collier, R. W., and Lilley, M. D. (1990). Chemical reaction rates and entrainment within the Endeavour Ridge hydrothermal plume. *Earth and Planetary Science Letters*, 99, pp. 315-335.

Kadko, D., Feely, R., and Massoth, G. (1994). Scavenging of ^{234}Th and phosphorus removal from the hydrothermal effluent plume over the North Cleft segment of the Juan de Fuca Ridge. *Journal of Geophysical Research: Solid Earth (1978–2012)*, 99(B3), pp. 5017-5024.

Kadko, D. (1996). Radioisotopic studies of submarine hydrothermal vents. *Reviews of Geophysics*, 34(3), pp. 349-366.

Klinkhammer, G., and Hudson, A. (1986). Dispersal patterns for hydrothermal plumes in the South Pacific using manganese as a tracer. *Earth and Planetary Science Letters*, 79(3), pp. 241-249.

Klunder, M. B., Laan, P., Middag, R., de Baar, H. J. W. and Bakker, K. (2012). Dissolved iron in the Arctic Ocean: Important role of hydrothermal sources, shelf input and scavenging removal. *Journal of Geophysical Research*, 117.

Klunder, M. B., Laan, P., Middag, R., De Baar, H. J. W. and Ooijen, J. V. (2011). Dissolved iron in the Southern Ocean (Atlantic sector). *Deep Sea Research Part II: Topical Studies in Oceanography*, 58, pp. 2678-2694.

Krishnaswami, S., Lal, D., Somayajulu, B. L. K., Weiss, R. F., Craig, H. (1976). Large volume in-situ filtration of deep Pacific waters: mineralogical and radioisotope studies. *Earth and Planetary Science Letters*, 32, pp. 420-429.

Luo, S. D., Ku, T. L., Kusakabe, M., Bishop, J. K. B., Yang, Y. L. (1995). Tracing particle cycling in the upper ocean with ^{230}Th and ^{228}Th: an investigation in the equatorial Pacific along 140°W. *Deep Sea Research Part II: Topical Studies in Oceanography*, 42(2), pp. 805-829.

Lupton, J. E., Craig, H. (1981). A major helium-3 source at 15°S on the East Pacific Rise. *Science*, 214(4516), pp. 13-18.

Lupton, J. E. (1995). Hydrothermal plumes: near and far field. *Seafloor hydrothermal systems: physical, chemical, biological, and geological interactions*, pp. 317-346.

Lupton J. E. (1998). Hydrothermal helium plumes in the Pacific Ocean. *Journal of Geophysical Research*, 103, pp. 15853-15868.

Lupton, J. E., Pyle, D. G., Jenkins, W. J., Greene, R., Evans, L. (2004). Evidence for an extensive hydrothermal plume in the Tonga-Fiji region of the South Pacific. *Geochemistry, Geophysics, Geosystems*, 5(1).

Lyle, M. W. (1986). Major element composition of leg-92 sediments. *Initial Reports of the Deep Sea Drilling Project*, 92, pp. 355-370.

Lyle, M., Leinen, M., Owen, R. M., Rea, D. K. (1987). Late Tertiary history of hydrothermal deposition at the East Pacific Rise, 19 degrees S; correlation to volcano-tectonic events. *Geophysical Research Letters*, 14(6), pp. 595-598.

Lyle, M., Marcantonio, F., Moore, W. S., Murray, R. W., Huh, C. A., Finney, B. P., and Mix, A. C. (2014). Sediment size fractionation and focusing in the equatorial Pacific: Effect on ^{230}Th normalization and paleoflux measurements. *Paleoceanography*, 29(7), pp. 747-763.

Mahowald, N. M., Baker, A. R., Bergametti, G., Brooks, N., Duce, R. A., Jickells, T. D., Kubilay, N., Prospero, J. M. and Tegen, I. (2005). Atmospheric global dust cycle and iron inputs to the ocean. *Global Biogeochemical Cycles*, 19(4).

Mahowald, N. M., Yoshioka, M., Collins, W. D., Conley, A. J., Fillmore, D. W., Coleman, D. B. (2006). Climate response and radiative forcing from mineral aerosols during the last glacial maximum, pre-industrial, current and doubled-carbon dioxide climates. *Geophysical Research Letters*, 33(20).

Mahowald, N. M., Engelstaedter, S., Luo, C., Sealy, A., Artaxo, P., Benitez-Nelson, C., Siefert, R. L. (2009). Atmospheric iron deposition: Global distribution, variability, and human perturbations*. *Marine Science*, 1.

Malahoff, A., Kolotyrkina, I. Y., Midson, B. P., Massoth, G. J. (2006). A decade of exploring a submarine intraplate volcano: Hydrothermal manganese and iron at Loihi volcano, Hawai'i. *Geochemistry, Geophysics, Geosystems*, 7(6).

Marchal, O., François, R., Stocker, T. F., Joos, F. (2000). Ocean thermohaline circulation and sedimentary $^{231}Pa/^{230}Th$ ratio. *Paleoceanography*, 15, pp. 625-641.

Martin, J. H., Gordon, R. M., Fitzwater, S. E. (1990). Iron in Antarctic waters, *Nature*, 345, pp. 156-158.

McGee, D., Marcantonio, F., Lynch-Stieglitz, J. (2007). Deglacial changes in dust flux in the eastern equatorial Pacific. *Earth and Planetary Science Letters*, 257, pp. 215-230.

Measures, C. I., Edmond, J. M. (1988). Aluminium as a tracer of the deep outflow from the Mediterranean. *Journal of Geophysical Research: Oceans (1978–2012)*, 93(C1), pp. 591-595.

Moore, J. K., Braucher, O. (2008). Sedimentary and mineral dust sources of dissolved iron to the world ocean. *Biogeosciences*, 5, pp. 631-656.

Moran, S. B., Hoff, J. A., Buesseler, K. O., Edwards, R. L. (1995). High precision ^{230}Th and ^{232}Th in the Norwegian Sea and Denmark by thermal ionization mass spectrometry. *Geophysical Research Letters*, 22, pp. 2589-2592.

Moran, S. B., Charette, M. A., Hoff, J. A., Edwards, R. L., Landing, W. M. (1997). Distribution of ^{230}Th in the Labrador Sea and its relation to ventilation. *Earth and Planetary Science Letters*, 150, pp. 151-160.

Moran, S. B., Shen, C. C., Weinstein, S. E., Hettinger, L. H., Hoff, J. H., Edmonds, H. N., Edwards, R. L. (2001). Constraints on deep water age and particle flux in the Equatorial and South Atlantic Ocean based on seawater ^{231}Pa and ^{230}Th data. *Geophysical Research Letters*, 28, pp. 3437-3440.

Moran, S. B., Shen, C. C., Edmonds, H. N., Weinstein, S. E., Smith, J. N., Edwards, R. L. (2002). Dissolved and particulate ^{231}Pa and ^{230}Th in the Atlantic Ocean: constraints on intermediate/deep water age, boundary scavenging, and ^{231}Pa/^{230}Th fractionation. *Earth and Planetary Science Letters*, 203, pp. 999-1014.

Nozaki, Y., Horibe, Y., Tsubota, H. (1981). The water column distributions of thorium isotopes in the western North Pacific. *Earth and Planetary Science Letters*, 54, pp. 203-216.

Nozaki, Y., Horibe Y. (1983). Alpha-emitting thorium isotopes in northwest Pacific deep waters, *Earth and Planetary Science Letters*, 65, pp. 39-50.

Nozaki, Y., and Nakanishi, T. (1985). ^{231}Pa and ^{230}Th profiles in the open ocean water column. *Deep Sea Research Part A. Oceanographic Research Papers*, 32(10), pp. 1209-1220.

Nozaki, Y., Yang, H. S., Yamada, M. (1987). Scavenging of Thorium in the ocean. *Journal of Geophysical Research: Oceans*, 92(C1), pp. 772-778.

Okubo, A., Obata, H., Gamo, T., and Yamada, M. (2012). ^{230}Th and ^{232}Th distributions in mid-latitudes of the North Pacific Ocean: effect of bottom scavenging. *Earth and Planetary Science Letters*, 339, pp. 139-150.

Rea, D. K., Leinen, M., Janecek, T. R. (1985). Geologic approach to the long-term history of atmospheric circulation, *Science*, 227, pp. 721-725.

Roy-Barman, M., Chen, J. H., Wasserburg, G. J. (1996). Th-230–Th-232 systematics in the central Pacific Ocean: the sources and the fates of thorium. *Earth and Planetary Science Letters*, 139(3-4), pp. 351-363.

Roy-Barman, M., Coppola, L., Souhaut, M. (2002). Thorium isotopes in the western Mediterranean Sea: an insight into the marine particle dynamics. *Earth and Planetary Science Letters*, 196, pp. 161-174.

Roy-Barman, M. (2009). Modelling the effect of boundary scavenging on Thorium and Protactinium profiles in the ocean. *Biogeosciences*, 6, pp. 1853-7896.

Santschi, P. H., Murray, J. W., Baskaran, M., Benitez-Nelson, C. R., Guo, L. D., Hung, C. C., Lamborg, C., Moran, S. B., Passow, U., Roy-Barman, M. (2006). Thorium speciation in seawater. *Marine Chemistry*, 100, pp. 250-268.

Scholten, J. C., Rutgers van der Loeff, M. M., Michel, A. (1995). Distribution of ^{230}Th and ^{231}Pa in the water column in relation to the ventilation of the deep Arctic basins. *Deep Sea Research Part II: Topical Studies in Oceanography*, 42(6), 1519-1531.

Scholten, J. C., Fietzke, J., Mangini, A., Stoffers, P., Rixen, T., Gaye-Haake, B., and Ittekkot, V. (2005). Radionuclide fluxes in the Arabian Sea: the role of particle composition. *Earth and Planetary Science Letters*, 230(3–4), pp. 319-337.

Singh, A. K., Marcantonio, F., Lyle, M. (2011). Sediment focusing in the Panama Basin, Eastern Equatorial Pacific Ocean. *Earth and Planetary Science Letters*, 309 (1–2), pp. 33-44.

Singh, A. K., Marcantonio, F., Lyle, M. (2013). Water column ^{230}Th systematics in the eastern equatorial Pacific Ocean and implications for sediment focusing. *Earth and Planetary Science Letters*, 362, pp. 294-304.

Spencer, D. W., Bacon, M. P., Brewer, P. G. (1981). Models of the distribution of ^{210}Pb in a section across the north equatorial Atlantic Ocean. *Journal of Marine Research*, 39, pp. 119-138.

Taylor, S. R. and McLennan, S. M. (1995). The geochemical evolution of the continental crust. *Reviews of Geophysics*, 33, pp. 241-265.

Trefry, J. H., Metz, S. (1989). Role of hydrothermal precipitates in the geochemical cycling of vanadium, *Nature*, 342, pp. 531-533.

Trocine, R. P., Trefry, J. H. (1988). Distribution and chemistry of suspended particles from an active hydrothermal vent site on the Mid-Atlantic Ridge at 26°N, *Earth and Planetary Science Letters*, 88, pp. 1-15.

Van der Loeff, M. M. R., Berger, G. W. (1993). Scavenging of Th-230 and Pa-231 near the Antarctic Polar Front in the South-Atlantic. *Deep Sea Research Part I: Oceanographic Research Papers*, 40(2), pp. 339-357.

Venchiarutti, C., Jeandel, C., Roy-Barman, M. (2008). Particle dynamics study in the wake of Kerguelen Island using thorium isotopes. *Deep Sea Research Part I: Oceanographic Research Papers*, 55(10), pp. 1343-1363.

Wang, C., Jeong, G. R., Mahowald, N. (2009). Particulate absorption of solar radiation: anthropogenic aerosols vs. dust. *Atmospheric Chemistry and Physics*, 9, pp. 3935–3945.

Watson, A. J., Bakker, D. C. E., Ridgwell, A. J., Boyd, P. W., Law, C. S. (2000). Effect of iron supply on Southern Ocean CO_2 uptake and implications for glacial atmospheric CO_2. *Nature*, 407, pp. 730-733.

Winckler, G., Anderson, R. F., Fleisher, M. Q., McGee, D., Mahowald, N. M. (2008). Covariant glacial-interglacial dust fluxes in the Equatorial Pacific and Antarctica. *Science*, 320, pp. 93-96.

Woodard, S. C., Thomas, D. J., Marcantonio, F. (2012). Thorium-derived dust fluxes to the tropical Pacific Ocean, 58 Ma. *Geochimica et Cosmochimica Acta*, 87, pp. 194-209.

Wu, J., Wells, M. L., Rember, R. (2011). Dissolved iron anomaly in the deep tropical–subtropical Pacific: Evidence for long-range transport of hydrothermal iron. *Geochimica et Cosmochimica Acta*, 75(2), pp. 460-468.

Yu, E. F., Francois, R., Bacon, M. P., Fleer, A. P. (2001). Fluxes of ^{230}Th and ^{231}Pa to the deep sea: implications for the interpretation of excess ^{230}Th and ^{231}Pa/^{230}Th profiles in sediments. *Earth and Planetary Science Letters*, 191, pp. 219-230.